Sensitivity Gaussian packets

Luděk Klimeš

Department of Geophysics, Faculty of Mathematics and Physics, Charles University, Ke Karlovu 3, 121 16 Praha 2, Czech Republic (http://sw3d.cz/staff/klimes.htm)

Received: April 24, 2021; Revised: August 2, 2021; Accepted: September 14, 2021

ABSTRACT

Perturbations of elastic moduli and density can be decomposed into Gabor functions. The wave field scattered by the perturbations is then composed of waves scattered by the individual Gabor functions. The scattered waves can be estimated using the first–order Born approximation with the paraxial ray approximation. For a particular source generating a short–duration broad–band incident wave field with a smooth frequency spectrum, each Gabor function generates at most a few scattered sensitivity Gaussian packets propagating in determined directions. Each of these scattered Gaussian packets is sensitive to just a single linear combination of the perturbations of elastic moduli and density corresponding to the Gabor function. This information about the Gabor function is lost if the scattered sensitivity Gaussian packet does not fall into the aperture covered by the receivers and into the recording frequency band. We illustrate this loss of information using the difference between the 2–D Marmousi model and the corresponding smooth velocity model. We decompose the difference into Gabor functions. For each of the 240 point shots, we consider 96 receivers. For each shot and each Gabor function, we trace the central ray of each sensitivity Gaussian packet. If a sensitivity Gaussian packet arrives to the receiver array within the recording time interval and frequency band, the recorded wave field contains information on the corresponding Gabor function. We then decompose the difference into the part influencing some recorded seismograms, and the part on which we recorded no information and which thus cannot be recovered from the reflection experiment.

Keywords: wave-field inversion, elastic waves, elastic moduli, seismic anisotropy, heterogeneous media, perturbation

Stud. Geophys. Geod., 65 (2021), 296–304, DOI: 10.1007/s11200-021-0931-x

1. INTRODUCTION

Klimeš (2012) studied how the perturbations of a generally heterogeneous isotropic or anisotropic structure manifest themselves in the wave field, and which perturbations can be detected within a limited aperture and a limited frequency band. He considered a smoothly varying heterogeneous generally anisotropic background medium, with an isotropic background medium as a special case. He considered generally anisotropic perturbations of the medium, with isotropic perturbations as a special case. He decomposed the perturbations of elastic moduli and density into Gabor functions, and approximated the waves scattered by individual Gabor functions analytically using the Born approximation with high–frequency approximations. For a particular source generating a short–duration broad–band incident wave field with a smooth frequency spectrum, each Gabor function generates at most a few scattered *sensitivity Gaussian packets* propagating in determined directions. Each of these scattered Gaussian packets is sensitive to just a single linear combination of the perturbations of elastic moduli and density corresponding to the Gabor function. This information about the Gabor function is lost if the scattered sensitivity Gaussian packet does not fall into the aperture covered by the receivers and into the recording frequency band.

In this paper, we illustrate this loss of information using the difference between the 2–D Marmousi model (*Versteeg and Grau, 1991*) and the corresponding smooth velocity model (*Klimeš, 2000*). We treat the difference as the perturbation of the smooth velocity model. We decompose the difference into Gabor functions according to *Klimeš (2008a, Sec. 2.3)*. For each of the 240 point shots, we consider 96 receivers (*Versteeg and Grau, 1991*). For each shot and each Gabor function, we trace the central ray of each sensitivity Gaussian packet. If a sensitivity Gaussian packet arrives to the receiver array within the recording time interval and frequency band, the recorded wave field contains information on the corresponding Gabor function. We then decompose the difference into the part influencing some recorded seismograms, and the part on which we recorded no information and which thus cannot be recovered from the reflection experiment.

In Section 2, we briefly summarize the decomposition of the perturbations into Gabor functions, and basic information on the sensitivity Gabor functions generated by the Gabor functions. Section 3 is then devoted to the numerical example.

2. STRUCTURAL GABOR FUNCTIONS AND SENSITIVITY GAUSSIAN PACKETS

2.1. Gabor representation of medium perturbations

We consider infinitesimally small perturbations $\delta c_{ijkl}(\mathbf{x})$ and $\delta\varrho(\mathbf{x})$ of elastic moduli $c_{ijkl}(\mathbf{x})$ and density $\varrho(\mathbf{x})$. We decompose the perturbations into Gabor functions $g^\alpha(\mathbf{x})$ indexed by α:

$$\delta c_{ijkl}(\mathbf{x}) = \sum_\alpha \delta c^\alpha_{ijkl}\; g^\alpha(\mathbf{x}) \quad , \qquad \delta\varrho(\mathbf{x}) = \sum_\alpha \delta\varrho^\alpha g^\alpha(\mathbf{x}) \quad , \tag{1}$$

$$g^\alpha(\mathbf{x}) = \exp[\mathrm{i}\mathbf{k}^{\alpha\,\mathrm{T}}(\mathbf{x}-\mathbf{x}^\alpha) - \tfrac{1}{2}(\mathbf{x}-\mathbf{x}^\alpha)^{\mathrm{T}}\mathbf{K}^\alpha(\mathbf{x}-\mathbf{x}^\alpha)] \quad . \tag{2}$$

Gabor functions $g^\alpha(\mathbf{x})$ are centred at various spatial positions $\mathbf{x}^\alpha$ and have various structural wavenumber vectors $\mathbf{k}^\alpha$. We assume here equal Gabor functions $g^\alpha(\mathbf{x})$ for all elastic moduli and density at each phase–space position α.

To decompose any function from a Hilbert space of functions defined in the velocity–model volume, Gabor functions $g^\alpha(\mathbf{x})$ should form a frame in the Hilbert space (*Daubechies, 1992*). Finding such a frame need not be a simple task if matrix $\mathbf{K}^\alpha$ varies with α. Note that the infinite number of Gabor functions forming the frame can be reduced to a finite number, because the maximum source frequency or maximum recording frequency implies the maximum norm of structural wavenumber vector $\mathbf{k}^\alpha$ for scattering.

The wave field scattered by the perturbations is composed of waves $\delta u_i^\alpha(\mathbf{x},t)$ scattered by individual Gabor functions:

$$\delta u_i(\mathbf{x},t) = \sum_\alpha \delta u_i^\alpha(\mathbf{x},t) \quad . \tag{3}$$

To calculate scattered waves $\delta u_i^\alpha(\mathbf{x},t)$, we apply several approximations.

2.2. Applied approximations

We assume that a short–duration broad–band wave field with a smooth frequency spectrum, incident at the location of the Gabor function, can be expressed in terms of the amplitude and travel time. We approximate each wave $\delta u_i^\alpha(\mathbf{x},t)$ scattered by one Gabor function by the *first–order Born approximation*, which describes exactly the first–order sensitivity of the wave field to infinitesimally small structural perturbations. We apply the *ray–theory approximation* (*Červený, 2001*) to the Green tensor in the Born approximation. We use the *high–frequency approximation of spatial derivatives* of both the incident wave and the Green tensor. In this high–frequency approximation, we neglect the derivatives of the amplitude, which are of order $1/$*frequency* with respect to the derivatives of the travel time. We make use of the *paraxial ray approximation* of the incident wave in a vicinity of central point $\mathbf{x}^\alpha$ of the Gabor function, and of the *two–point paraxial ray approximation* of the Green tensor at point $\mathbf{x}^\alpha$ and at the receiver. The paraxial ray approximation consists in a constant amplitude and in the second–order Taylor expansion of the travel time. The above mentioned approximations enable us to calculate wave $\delta u_i^\alpha(\mathbf{x},t)$, scattered by the Gabor function, analytically (*Klimeš, 2012*).

2.3. Sensitivity Gaussian packets

Considering the above approximations, wave $\delta u_i^\alpha(\mathbf{x},t)$ scattered by one Gabor function is composed of a few (i.e., 0 to 5 as a rule) Gaussian packets (*Klimeš, 2012*). Each of these sensitivity Gaussian packets has a specific frequency and propagates from point $\mathbf{x}^\alpha$ in a specific direction, see Fig. 1. The frequency (*Klimeš, 2012, Eq. 90*) and propagation direction (*Klimeš, 2012, Eq. 91*) depend on the direction of the incident wave and on the structural wavenumber vector $\mathbf{k}^\alpha$ of the Gabor

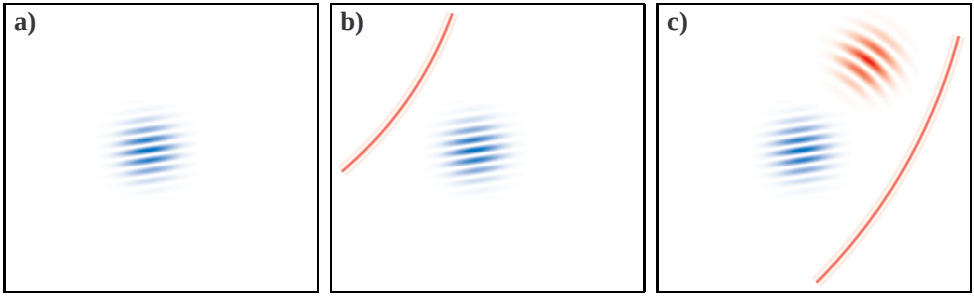

Fig. 1. Scattering at a single Gabor function. **a)** A single Gabor function $g^\alpha(\mathbf{x})$ centred at point $\mathbf{x}^\alpha$. **b)** Broad–band wave incident at the Gabor function. **c)** Scattered wave $\delta u_i^\alpha(\mathbf{x}, t)$.

function. The sensitivity Gaussian packet has non–zero amplitude if its frequency falls into the source frequency band. Each of these sensitivity Gaussian packets scattered by Gabor function $g^\alpha(\mathbf{x})$ is sensitive to just a single linear combination

$$\sum_{ijkl} \delta c^\alpha_{ijkl}\, E_i\, P_j\, e_k\, p_l - \delta\varrho^\alpha \sum_i E_i\, e_i \quad . \tag{4}$$

of perturbation coefficients δc^α_{ijkl} and $\delta\varrho^\alpha$ corresponding to the Gabor function (*Klimeš, 2012, Eq. 68*). Here P_i and E_i are the components of the slowness vector and of the unit polarization vector of the incident wave, and p_i and e_i are the components of the slowness vector and of the unit polarization vector of the sensitivity Gaussian packet. This information about the Gabor function is lost if the sensitivity Gaussian packet does not fall into the aperture covered by the receivers and into the recording frequency band. The situation improves with the increasing number of differently positioned sources. If we have many sources, the sensitivity Gaussian packets propagating from a Gabor function may be lost during the measurement corresponding to one source, but recorded during the measurement corresponding to another, differently positioned source. However, the problem is not only to record the sensitivity Gaussian packets from a Gabor function, but to record them in as many different measurement configurations as to resolve perturbation coefficients δc^α_{ijkl} and $\delta\varrho^\alpha$.

3. MARMOUSI EXAMPLE

We consider the distribution of the P–wave velocity in the Marmousi structure (*Versteeg and Grau, 1991*), see Fig. 2. The velocity model for ray tracing must be smooth and is displayed in Fig. 3. The velocity model (*Bucha and Bulant, 2019*) was smoothed by *Klimeš (2000)*, refer to *Žáček (2002)* for more details. The velocity difference between the Marmousi structure and the velocity model is displayed in Fig. 4.

For the decomposition of the velocity difference, we generate the set of Gabor functions $g^\alpha(\mathbf{x})$ with matrices $\mathbf{K}^\alpha$ optimized according to *Klimeš (2008b)*. We obtain 67014 Gabor functions within the selected wavenumber domain. Refer to

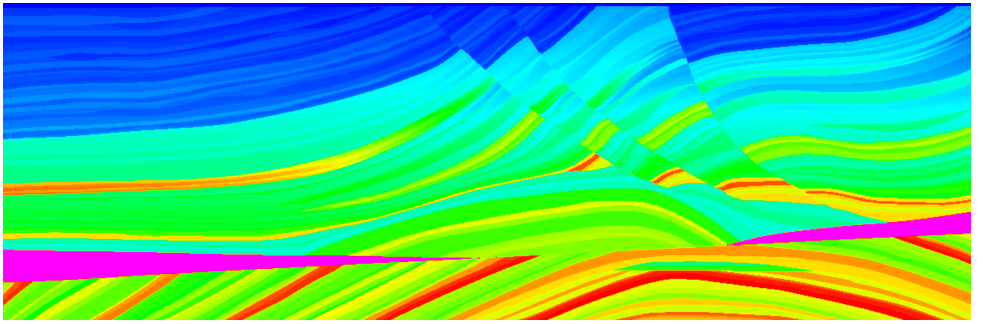

Fig. 2. P–wave velocity in the Marmousi structure. Blue correponds to 1500 m/s, yellow correponds to 3900 m/s, magenta correponds to 5500 m/s. The velocity–model area displayed in Figs 2–8 extends for 9204 m horizontally and 3004 m vertically.

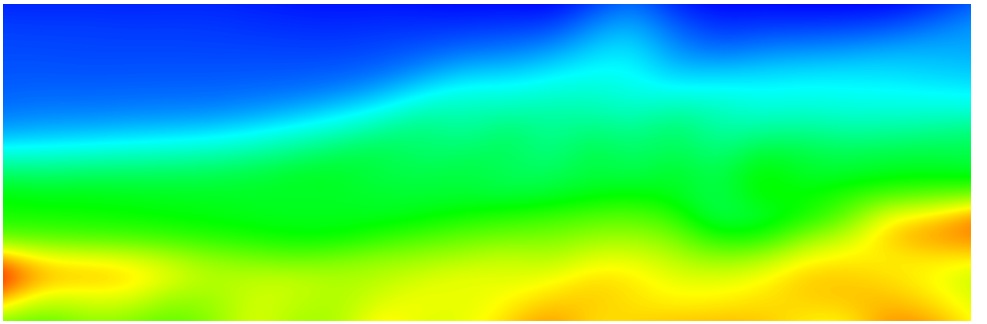

Fig. 3. P–wave velocity in the velocity model for ray tracing. The same colour scale as in Fig. 2.

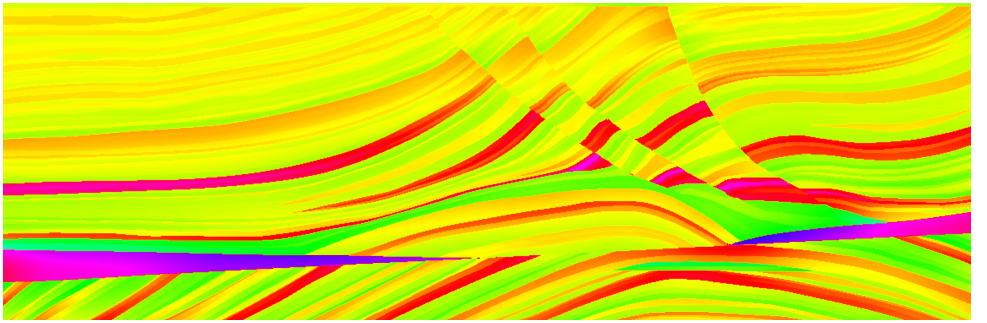

Fig. 4. Velocity difference between the Marmousi structure and the velocity model. Yellow correponds to 0 m/s, red correponds to 800 m/s, green correponds to -800 m/s.

Fig. 5 for 14 selected Gabor functions. We then decompose the velocity difference from Fig. 4 into the sum of Gabor functions according to *Klimeš (2008a, Sec. 2.3)*. For each shot, we calculate the quantities describing the paraxial approximation

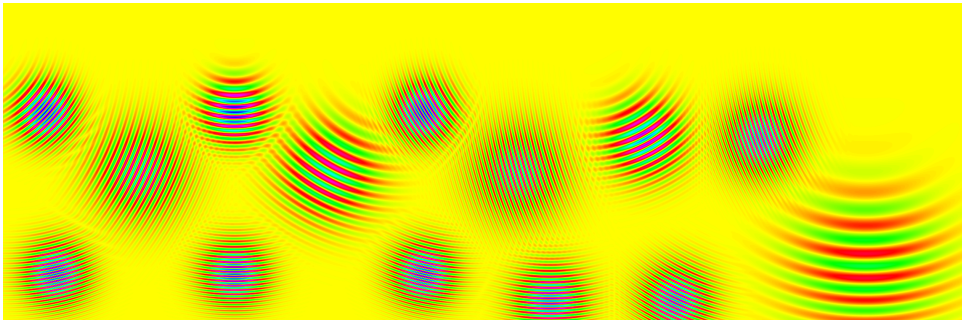

Fig. 5. Example showing 14 of 67014 optimized Gabor functions used to decompose the velocity difference.

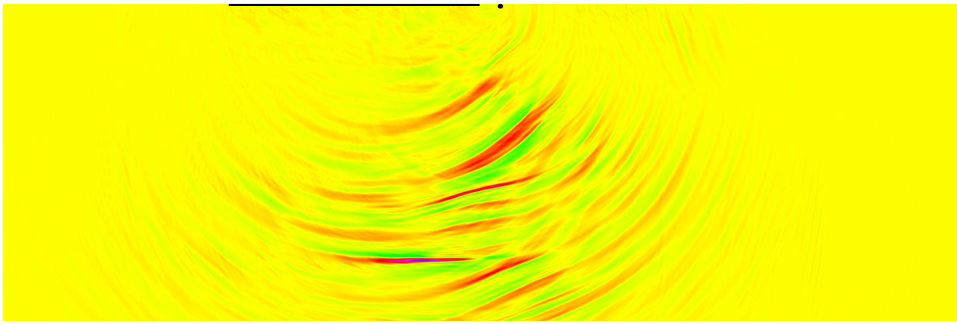

Fig. 6. Sum of the Gabor functions influencing the seismograms recorded for shot 70. The black dot and line correspond to the source and receiver points, respectively. The same colour scale as in Fig. 4.

of the incident P wave at all central points of Gabor functions using the controlled initial–value ray tracing (*Bulant, 1999*) followed by the interpolation within ray cells (*Bulant and Klimeš, 1999*). For each shot and each Gabor function, we calculate the initial conditions for the corresponding sensitivity Gaussian packets which form the scattered wave (*Klimeš, 2012, Eqs 90–91*). We consider sensitivity Gaussian packets corresponding to the given frequency band only. We then trace the central ray of each sensitivity Gaussian packet using the initial–value ray tracing (*Červený, Klimeš and Pšenčík, 1988*). If a sensitivity Gaussian packet arrives to the receiver array within the recording time interval and frequency band, the recorded wave field contains information on the corresponding Gabor function. The sum of the Gabor functions influencing the seismograms recorded for shot 70 is displayed in Fig. 6. We consider here all Gabor functions sensitive to at least one linear combination of perturbations.

The velocity difference from Fig. 4 can be decomposed into the part to which the recorded seismograms are not sensitive and into the part to which the recorded seismograms are sensitive. The sum of 44924 Gabor functions influencing the seismograms collected from all shots is displayed in Fig. 7. This is the part

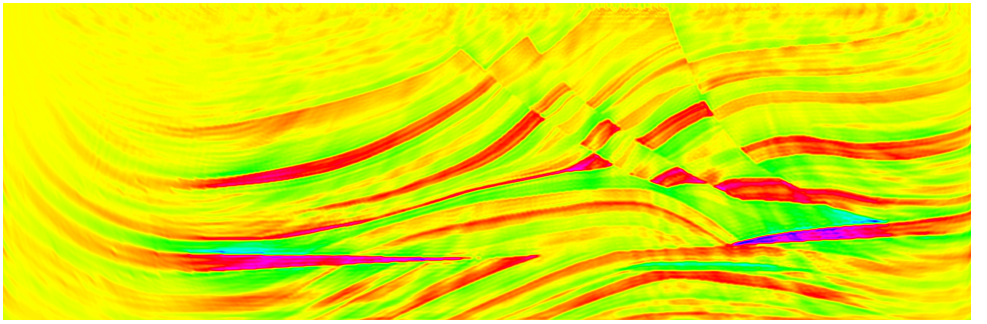

Fig. 7. Sum of the Gabor functions influencing the seismograms collected from all shots. The same colour scale as in Fig. 4.

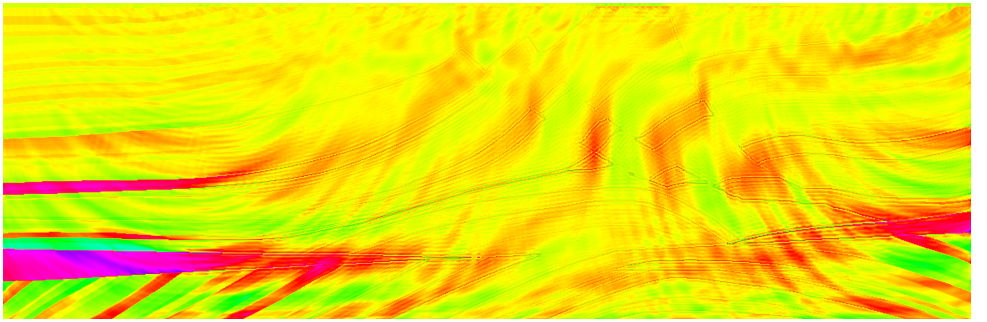

Fig. 8. Part of the velocity difference from Fig. 4 influencing no recorded seismogram. The same colour scale as in Fig. 4.

of the velocity difference to which the recorded seismograms are sensitive. The remaining part of the velocity difference, influencing no recorded seismogram within the first–order Born approximation, is displayed in Fig. 8. This part of the velocity difference cannot be recovered from the Marmousi seismograms.

4. COMPUTATIONAL COST

The computational cost mostly consists in decomposing the given structure into the Gabor functions, which represents the solution of the ill–conditioned system of linear equations with the minimum squared norm (*Klimeš, 2008a, Eqs 21–22*). The numbers of both unknowns and equations are equal to the number of the Gabor functions. The system matrix is symmetric and sparse.

In the simple 2–D presented example, we have 67014 equations for 67014 unknowns. The ratio of non–zero elements of the sparse symmetric matrix is 0.00341.

5. CONCLUSIONS

Perturbations of elastic moduli and density can be decomposed into Gabor functions. A short–duration broad–band wave with a smooth frequency spectrum incident at the location of each Gabor function generates at most a few scattered sensitivity Gaussian packets. Each sensitivity Gaussian packet has a specific frequency and propagates in a specific direction. Refer to *Klimeš (2012)* for the relevant equations. Each Gaussian packet is sensitive to a single linear combination of the perturbations of elastic moduli and density corresponding to the Gabor function. This information about the Gabor function is lost if the sensitivity Gaussian packet does not fall into the aperture covered by the receivers and into the recording frequency band. We can thus see which details of the underlying geological structure cannot be recovered with a given acquisition geometry.

This loss of information is demonstrated in Figs 7 and 8 using the difference between the 2–D Marmousi model (*Versteeg and Grau, 1991*) and the corresponding smooth velocity model (*Klimeš, 2000*). The proposed technique can be valuable for evaluating the resolution limitations of inverting a particular reflection seismic survey.

In this way, we can compare several geometries of reflection seismic surveys. For each geometry, we decompose a testing structure analogous to Fig. 4 into the part influencing the seismograms and the part influencing no recorded seismogram, analogously to Figs 7 and 8. We may then observe how to improve a given acquisition geometry for better inversion results.

The sensitivity Gaussian packets can enable to replace migration by true linearized inversion of reflection seismic data. For the algorithm of the linearized inversion of the complete set of seismograms recorded for all shots, refer to *Klimeš (2008a)*.

Acknowledgements: The suggestions by David Henley and an anonymous reviewer made it possible for me to improve the paper considerably. The research has been supported by the Czech Science Foundation under contract 21-15272J, and by the members of the consortium "Seismic Waves in Complex 3–D Structures" (see "http://sw3d.cz").

References

Bucha V. and Bulant P. (Eds), 2019. SW3D–CD–23 (DVD–ROM). *Seismic Waves In Complex 3–D Structures*, **29**, 71–72 (online at "http://sw3d.cz")

Bulant P., 1999. Two–point ray–tracing and controlled initial–value ray–tracing in 3–D heterogeneous block structures. *J. Seism. Explor.*, **8**, 57–75

Bulant P. and Klimeš L., 1999. Interpolation of ray theory traveltimes within ray cells. *Geophys. J. Int.*, **139**, 273–282

Červený V., 2001. *Seismic Ray Theory.* Cambridge Univ. Press, Cambridge, U.K.

Červený V., Klimeš L. and Pšenčík I., 1988. Complete seismic–ray tracing in three–dimensional structures. In: Doornbos, D.J. (Ed.), *Seismological Algorithms.* Academic Press, New York, 89–168

Daubechies I., 1992. *Ten Lectures on Wavelets.* SIAM, Philadelphia, PA.

Klimeš L., 2000. Smoothing the Marmousi model for Gaussian–packet migrations. *Seismic Waves In Complex 3–D Structures*, **10**, 63–74 (online at "http://sw3d.cz")

Klimeš L., 2008a. Stochastic wavefield inversion using the sensitivity Gaussian packets. In: *Seismic Waves in Complex 3–D Structures, Report 18.* Dep. Geophys., Charles Univ., Prague, 71–85 (online at "http://sw3d.cz")

Klimeš L., 2008b. Optimization of the structural Gabor functions in a homogeneous velocity model for a zero–offset surface seismic reflection survey. In: *Seismic Waves in Complex 3–D Structures, Report 18.* Dep. Geophys., Charles Univ., Prague, 115–127 (online at "http://sw3d.cz")

Klimeš L., 2012. Sensitivity of seismic waves to structure. *Stud. Geophys. Geod.*, **56**, 483–520

Versteeg R.J. and Grau G. (Eds), 1991. The Marmousi experience. In: *Proc. EAGE workshop on Practical Aspects of Seismic Data Inversion (Copenhagen, 1990).* Eur. Assoc. Explor. Geophysicists, Zeist

Žáček K., 2002. Smoothing the Marmousi model. *Pure Appl. Geophys.*, **159**, 1507–1526